

Nature of the $\text{Cu}^+ - \text{NO}$ Bond in the Gas Phase and at Different Types of Cu^+ Sites in Zeolite Catalysts

Markéta Davidová, Dana Nachtigallová, and Petr Nachtigall*

Institute of Organic Chemistry and Biochemistry, Academy of Sciences of the Czech Republic and Center for Complex Molecular Systems and Biomolecules, Flemingovo n. 2, 166 10, Prague 6, Czech Republic

Joachim Sauer

Humboldt-Universität, Institut für Chemie, Unter den Linden 6, 10099 Berlin, Germany

Received: May 21, 2004; In Final Form: July 2, 2004

The activation of Cu^+ ions for NO binding by the zeolite “ligand” is analyzed. Density functional theory (DFT) calculations show that the interaction of NO with isolated Cu^+ ions and with Cu^+ ions in zeolites is of different character. In gas-phase $\text{Cu}^+ - \text{NO}$ complexes interactions of the a' singly occupied orbital (SOMO) on NO with the unoccupied 4s and the occupied 3d orbitals on Cu^+ depopulate the antibonding SOMO and this strengthens the NO bond. In the Cu/zeolite system electrostatic attraction increases the Pauli repulsion and pushes up the (occupied) 3d orbitals, which can interact with the a'' LUMO of NO. This interaction populates the antibonding LUMO of NO and, hence, weakens the NO bond. The binding of NO onto Cu^+ sites in high-silica zeolites MFI and FER is investigated by the combined quantum mechanics/interatomic potential function approach that describes the particular framework topology. Two types of Cu^+ sites are studied, on the channel wall (coordination to 3–4 framework O atoms) and on the channel intersection (coordination to 2 O atoms). Upon the interaction with NO the Cu^+ ion stays coordinated to only two framework oxygen atoms belonging to the AlO_4 tetrahedron and the structures of all ON–Cu/zeolite adsorption complexes become very similar. EPR hyperfine coupling constants (HFCC) were calculated and compared with experiment. The isotropic component of HFCC strongly depends on CuNO angle, but due to small variations of this angle, it will be difficult to resolve EPR signals (or other spectroscopic signals) for different sites. The interaction of NO with the Cu^+ sites on the channel intersection is significantly stronger (29.5–27.1 kcal/mol) than the interaction with the Cu^+ sites on the channel wall (22.6–15.0 kcal/mol) because framework deformation into a state prepared for bonding NO costs (deformation) energy.

1. Introduction

When embedded into a zeolite matrix, transition metal ions show high catalytic activity and selectivity, while in the gas phase the same ions are either not active or undergo different reactions. For example, Fe-exchanged zeolites are selective catalysts in arene oxygenation with N_2O and the active species has been identified as FeO_2^+ .¹ In contrast, in the gas-phase FeO_2^+ and benzene do not yield phenol, but undergo ligand exchange and charge exchange.² The present study deals with Cu-exchanged zeolites, Cu/MFI in particular, which shows high catalytic activity in direct NO_x decomposition,^{3,4} while naked Cu^+ ions do not catalyze this reaction as shown by Koszinowski et al.⁵ Cu^+ complexes with organic $[\text{HB}(\text{tBu-pz})_3]^+$ and $[\text{HB}(\text{Me}_2\text{-pz})_3]^+$ ligands,^{6,7} which have the negative charge and the σ -donor sites in common with the zeolite matrix (three N sites replace the O sites of the zeolite framework) and bind NO and disproportionation reactions have been observed. This suggests that the unusual catalytic activity of transition-metal-exchanged zeolites must be due to activation of the transition-metal ion by the zeolite framework which functions as a specific ligand. Dramatic changes in Cu–ligand interaction upon insertion into a zeolite were clearly demonstrated for NO_2 interaction with the Cu/MFI system.⁸

The present study investigates the $\text{Cu}^+ - \text{zeolite}$ interaction with the aim to answer the more general question of how the ligand activates transition-metal ions for NO binding and subsequent reactions. Differently from homogeneous catalysis and from amorphous silicate matrixes, the complex structure of zeolite frameworks provides different, crystallographically well-defined “extraframework” sites to which the transition-metal ions may bind. The coordination of transition-metal ions may vary from site to site and the activity of different zeolite catalysts will depend on the distribution of these sites as a function of the framework topology. Two types of Cu^+ sites were identified in high-silica zeolites using various experimental techniques including EXAFS, IR, EPR, or UV–Vis.^{9–11} Details of the structure and coordination of Cu^+ in these two site types were proposed based on computational studies.^{12,13} In type I sites Cu^+ is coordinated to 3–4 oxygen atoms within the six-member aluminosilicate ring on the wall of one of the zeolite channels. In type II sites Cu^+ is coordinated to 2 oxygen atoms of an AlO_4 tetrahedron located on the intersection of two channels. Figure 1 shows type I and type II Cu^+ sites in zeolites MFI and FER.

It was shown that Cu^+ ions in different crystallographic sites have different abilities to bind additional ligands.^{14,15} The interaction of nitrogen oxides with $\text{Cu}^+ - \text{zeolite}$ systems was studied previously using small cluster models^{16–27} or using a

* To whom correspondence should be addressed. E-mail: petr.nachtigall@uochb.cas.cz.

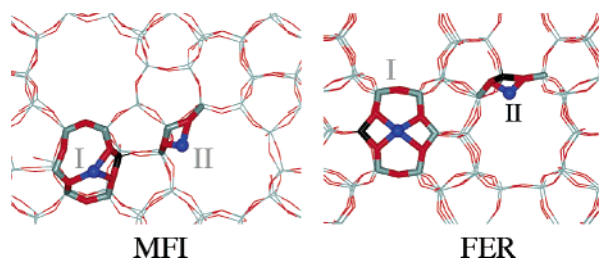


Figure 1. The Cu⁺ sites in MFI and FER. Type I and type II sites are located on the channel wall and on the channel intersection, respectively. For each structure, views along the main channel ((010) and (001) cut for MFI and FER, respectively) are shown.

combined quantum mechanics/interatomic potential function (QM-pot) technique.⁸ However, the effect of the zeolite topology and Cu⁺ ion coordination on the interaction with NO was not investigated. Hence, we examine the binding of NO onto different Cu⁺ sites in high-silica zeolites MFI and FER and compare it with the binding to gas-phase Cu⁺ ions. We would like to understand how structure and coordination of the transition-metal ions vary as a function of the crystallographic site and of the framework topology and how these changes do affect the reactivity. Calculated properties are compared with available experimental data; in particular, heats of adsorption and ESR hyperfine coupling constants (HFCC) are investigated for various Cu⁺ site types.

2. Systems Studied and Models Used

MFI was represented by a unit cell consisting of 96 atoms in tetrahedral sites (T atoms, 1 Al, 95 Si atoms), 192 framework O atoms, 1 Cu atom, and the NO molecule. FER was represented by a unit cell consisting of 72 T atoms (1 Al, 71 Si atoms), 144 framework O atoms, 1 Cu atom, and the NO molecule. Periodic boundary conditions were applied to the unit cell. Within the QM-pot approach, the inner part including the NO molecule, Cu⁺, and the selected zeolite framework atoms is embedded in the surrounding periodic zeolite framework (outer part). The dangling bonds of the inner part were saturated by H atoms connected to framework oxygen atoms. The inner part atoms and the link H atoms together form the cluster. Depending on the site type, clusters ranging from three (3-T model, ON–CuT₃O₂(OH)₈) to nine TO₄ units (9-T model, ON–CuT₉O₁₁(OH)₁₄) were adopted.

The size of the cluster model used for the description of the ON–CuZ system depends on the type of Cu⁺ ion site. The interaction of NO with type I sites in MFI is investigated for the previously defined sites¹³ Z6 (Al atom in T4 framework position) on the wall of the zigzag channel using the 6-T_r ring model (see Figure 3, top) and for the M7 site (Al atom in T7 position) on the wall of the main channel using the 7-T model (see Figure 4 in ref 13). The NO interaction with type I sites in FER was investigated for the P6 site on the wall of the perpendicular channel (Al atom in T1 position) using the 6-T_r model (see Figure 2 in ref 12). The interaction with Cu⁺ in type II sites was investigated with the 3-T model for both MFI and FER (see Figure 3 in ref 13) with the Al atom in T12 and T2 positions, respectively.

3. Calculations

The structures of ON–Cu⁺ zeolite adsorption complexes in MFI and FER zeolites were obtained by energy minimization using the combined quantum mechanics/interatomic potential function (QM-Pot) technique.²⁸ The cluster is treated at the DFT level employing the B3LYP^{29,30} exchange correlation functional.

TABLE 1: Isotropic Hyperfine Coupling Constants, A_0 , and Anisotropic Components of the shf Tensor, T_x , T_y , and T_z (in 10^{-4} cm⁻¹) for ON–CuMFI (Type II Site, I2, Al at T12) Calculated Using Various Exchange-Correlation Functionals and Basis Sets^a

		BP86 ^b	BPW91 ^b	BLYP ^b	B3LYP ^b	B3LYP ^c	BHLYP ^b
Cu	ρ^d	0.085	0.081	0.077	0.023	0.026	−0.011
Cu	A_0	189.4	186.9	181.2	147.4	149.3	116.1
	T_x	27.9	28.0	28.0	28.6	27.4	29.2
	T_y	−5.1	−5.0	−5.0	−4.9	−4.7	−6.1
	T_z	−22.8	−23.0	−23.0	−23.7	−22.7	−23.1
N	Al ^e	25.4	25.4	27.1	29.5	29.8	34.2

^a Calculations made on the 3-T cluster model at the QM-Pot optimized geometry for the embedded 3-T cluster. ^b Calculated with BS1 basis set. ^c Calculated with EPR basis set. ^d Mulliken spin population. ^e The largest value of the nitrogen hyperfine tensor corresponding to the direction determined by the $2\pi^*$ singly occupied orbital.

For the open shell systems, unrestricted Kohn–Sham calculations are made. Valence double- ζ -plus-polarization function basis sets were used for Cu, Si, Al, and H atoms and valence triple- ζ -plus-polarization function basis sets were used for O and N atoms.^{8,31} The outer part and the interactions between atoms of the inner and outer parts were described at the interatomic potential function (IPF) level, using the core–shell ion-pair potentials³² with parameters developed previously.^{13,33} The interaction of the NO molecule with the Cu⁺ ion is described at the DFT level. The interaction between the NO molecule and the zeolite framework is described by Lennard–Jones potentials with parameters derived from the universal force field.³⁴ The zero-point-vibrational energy (ZPVE) was calculated using the harmonic approximation and the basis set superposition error (BSSE) was calculated using the counterpoise correction method. It was found that ZPVE (0.9 kcal/mol) and BSSE (5.3 kcal/mol) do not depend on the Cu⁺ site; thus, the interaction energies were lowered by 6.2 kcal/mol for all sites considered in this study. The energy minimization of the structures have been carried out with the QM-pot program,²⁸ which makes the use of TURBODFT³⁵ and GULP³⁶ programs for DFT and shell model potential calculations, respectively.

The hyperfine coupling constants (HFCC) were calculated for the isolated Cu⁺NO complex and for the ON–CuZ adsorption complexes for one Cu site of each type, Z6 (type I) and I2 (type II). It is well-recognized that the calculated isotropic hyperfine coupling constant A_0 critically depends on the choice of the exchange and correlation functional, in particular, on the amount of mixing exact exchange into the functional.³⁷ A_0 as well as the anisotropic components of the shf tensor were calculated for the I2-site (3-T cluster model) using Becke exchange (B) functional and various gradient corrected correlation functionals, P86, PW91, and LYP, in particular. For the BLYP functional, the effect of admixture of an increasing amount of Fock exchange was studied, employing BLYP, B3LYP, and BHLYP functionals. Table 1 shows the results which confirm the previous analysis of Munzarová and Kaupp³⁷ of how HFCC for transition-metal compounds depend on the functional/basis set used. The anisotropic components of the shf tensors do not depend on the choice of the exchange correlation functional. On the contrary, the isotropic HFCC, A_0 , varies significantly with the choice of the functionals. In agreement with ref 37 A_0 calculated with the same exchange functional and various correlation functionals decreases in the order BP86 > PW91 > LYP from 189 to 181 $\times 10^{-4}$ cm⁻¹. With increasing admixture of exact exchange into the functional A_0 decreases significantly (181, 147, and 116 $\times 10^{-4}$ cm⁻¹ for BLYP, B3LYP, and BHLYP, respectively). Very recently, the

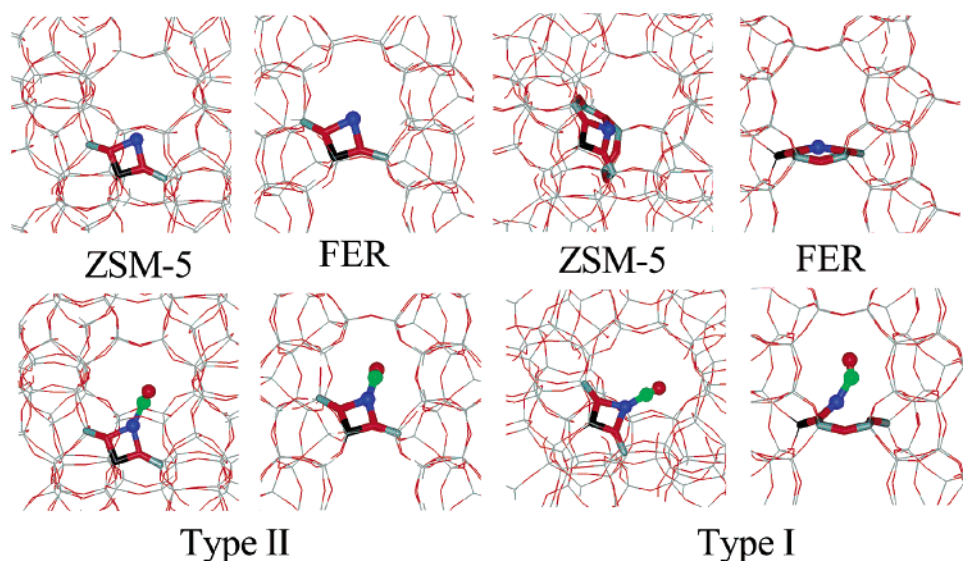


Figure 2. Coordination of the Cu^+ ions at type I and type II sites inside the MFI and FER frameworks before (top) and after (bottom) adsorption of the NO molecule. The Cu^+ ion and the atoms of NO are depicted as balls. Views along the direction of zigzag and perpendicular channels of MFI and FER, respectively.

dependence of hyperfine coupling constants on the functional and the basis set have been studied for $\text{Cu}^+ - \text{NO}$ by Freysoldt et al.³⁸ To assess the performance of the BS1 basis set, we calculated the HFCC constants at the B3LYP level employing a basis set recommended by Munzarová and Kaupp^{37,39} denoted EPR-BS. The results obtained with both basis sets are very similar (Table 1) and there is no need to go beyond our standard basis set for HFCC calculations. Neglect of relativistic corrections was found to underestimate the isotropic HFCC on Cu by less than 7%.^{37,40}

The final calculations were made at the B3LYP/BS1 level. For the type II site (I2) a 7-T cluster model was used at the QM-Pot optimized geometry for the embedded 3-T model. For the type I site (Z6) a 6-T_r model was used at the QM-Pot optimized geometry for the embedded 6-T_r model.

Atomic charges and spin populations were obtained from Mulliken and natural bond orbital (NBO) population analysis.⁴¹ The HFCC calculations as well as Mulliken and NBO population analysis used Gaussian03.⁴²

4. Results

4.1. Structure and Energies of NO Adsorbed on Different Cu^+ Sites in Zeolites. The interaction of NO with $\text{Cu}^+ - \text{zeolite}$ systems is examined for both types of Cu^+ sites inside the MFI and FER frameworks (Figure 1). As shown previously, the Cu^+ ion located on the wall of the channel (type I site) is coordinated to 3 or 4 framework oxygen atoms while the Cu^+ ion located on the channel intersection (type II site) is coordinated to only 2 framework oxygen atoms.^{12,13} Structures and coordinations of NO with the Cu^+ ion inside the zeolite channel system are depicted in Figure 2. After adsorption of NO onto the Cu^+ ions in zeolites, the structures of the adsorption complexes (lower part of Figure 2) are surprisingly similar regardless of the type of the original Cu^+ site, its location in the zeolite framework (see upper part of Figure 2), or the original local coordination of the Cu^+ ion to the framework. Upon interaction with the NO radical the Cu^+ ion keeps coordination to only two oxygen atoms of the AlO_4 tetrahedron (lower part of Figure 2). The coordination of the Cu^+ ion to two framework O atoms and to the nitrogen atom of NO is planar for type II sites and almost planar for type I sites (up to 22° deviation from planarity). This

is due to the fact that the location of type II sites inside the cavity at the channel intersection provides enough space for a planar coordination environment of the Cu^+ ion, while at type I sites the repulsive interaction between the channel walls and the NO ligand enforces a nonplanar coordination environment for the Cu^+ ion. For all adsorbate structures considered the $r(\text{Cu}-\text{O})$ bond lengths are in the range 2.02–2.08 Å. Also the $r(\text{Cu}-\text{N})$ bond lengths are very similar for all Cu^+ sites, 0.1 Å shorter than that for the gas-phase $\text{Cu}^+ - \text{NO}$ ion. The N–O bonds are in the range 1.158–1.161 Å, about 0.01 Å longer than that in the NO radical (1.148 Å), while in the gas-phase $\text{Cu}^+ - \text{NO}$ species the NO bond is 0.014 Å shorter than that in the NO radical. Correspondingly, the NO vibrational frequencies are also in a narrow range for all adsorbate structures (1776–1785 cm^{-1}) and compared to free NO (1876 cm^{-1}) shifted by 91–100 cm^{-1} to lower values, while in the $\text{Cu}^+ - \text{NO}$ complex this wavenumber is slightly blue-shifted (by 18 cm^{-1}). Observed wavenumbers are at 1812 cm^{-1} ,⁴³ about 64 cm^{-1} lower than the observed value for free NO. Better quantitative agreement can only be achieved if scale factors depending on the NO distance are used as shown for vibrations of CO adsorbed in Cu–zeolites.⁴⁴

Calculated interaction energies (including ZPVE and BSSE) as well as the most important geometrical parameters are summarized in Table 2. The adsorption energy is defined as negative energy of the reaction



The interaction of the NO molecule with the $\text{Cu}^+/\text{zeolite}$ is stronger for type II site ions than for type I site ions (Table 2). This corresponds to the changes of the Cu^+ coordination to the framework oxygen atoms upon the interaction with NO molecule. For both zeolites the energetically most stable adsorption complex is always located at the channel intersection (Figure 2). For type II sites the Cu^+ ion does not change its position and coordination significantly upon the interaction with NO (Figure 2). It is located near the channel intersection already before it binds the NO molecule. A rather different situation is observed for type I sites. The Cu^+ ion must lower its coordination to the framework in order to bind the NO molecule efficiently. The Cu^+ ion moves away from the channel wall

TABLE 2: Adsorption Energies and Geometrical Parameters of NO Adsorbed on Cu⁺ Sites in MFI and FER^a

zeolite	Cu ⁺ site	$E_{\text{int}}^{\text{BSSE}^b}$	E_{int}	E_{deform}^c	$R_{\text{Cu-O}}$	$r_{\text{Cu-N}}$	$r_{\text{O-N}}$	$\nu_{\text{O-N}}^f$	Cu ⁺ planar ^d	angle CuNO
MFI	I(M7)	22.6	27.9	7.0	2.06,2.06	1.807	1.159		7.9	149.8
	I(Z6)	22.3	27.6	8.3	2.03,2.05	1.809	1.159		12.2	148.5
	II(I2)	29.5	34.8	0.8	2.02,2.04	1.807	1.161	1776	1.4	145.7
FER	I(P6)	15.0	20.3	9.2	2.07,2.08	1.837	1.158	1785	21.7	140.8
	II(I2)	27.1	32.4	2.0	2.02,2.05	1.805	1.160	1782	0.0	148.4
naked Cu ⁺		27.3 ^e	30.8	—		1.934	1.134	1893		135.3

^a Corresponding values for gas-phase Cu⁺(NO) are also given. Energies are given in kcal/mol and bond lengths and angles are in Å and degrees, respectively. ^b BSSE correction (5.3 kcal/mol) included. ^c Zeolite framework deformation energy defined by eq 1a. ^d Deviation of Cu–N bond from the plane defined by Cu⁺ and two framework oxygen atoms coordinated to Cu⁺. ^e BSSE correction is 3.5 kcal/mol. ^f Calculated wavenumbers scaled by the ratio $\nu(\text{obsd})/\nu(\text{calcd}) = 1876/1970 = 0.9523$ for free NO. This ratio is close to the global B3LYP scale factor of 0.9614 (ref 58).

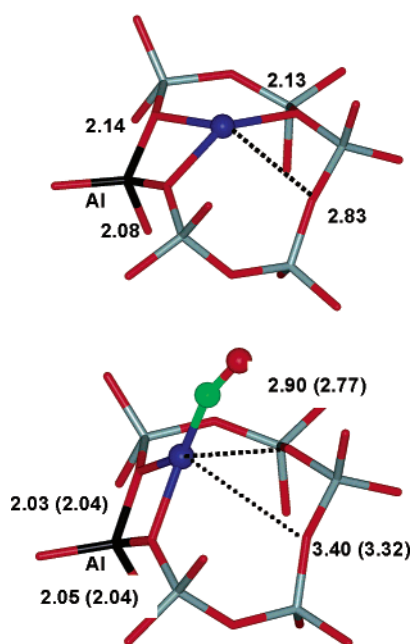
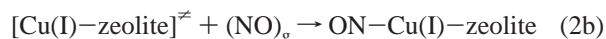
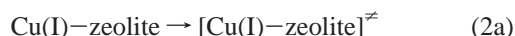


Figure 3. Structure and coordination of the type I Cu⁺ site in MFI (Z6 site, Al atom in T4 position) before (top) and after binding of NO (bottom). The Cu–O bond lengths (in Å) optimized at the QM-Pot level for the 6-T_R model are given. The bond lengths optimized at the QM-Pot level for the 3-T model are given in parentheses.

toward the channel intersection and it loses the coordination to non-AlO₄ framework oxygen atoms (Figure 2). Figure 3 shows details of the structural changes upon NO adsorption for the Z6 site on the wall of the zigzag channel of MFI. The loss of the coordination to the non-AlO₄ framework oxygen atoms is accompanied by the increase of the overall energy of the system. This behavior can be quantified by hypothetically splitting the NO adsorption process into two steps:



where [Cu(I)/zeolite][‡] denotes a hypothetical structure optimized for the interaction with the NO molecule (this hypothetical structure corresponds to the geometry depicted in Figure 3b but without the NO ligand). Therefore, eq 2a defines the “deformation” energy (E_{deform}) that the Cu⁺–zeolite system needs to adjust its structure for optimum NO binding. The net interaction energy of NO with the Cu⁺–zeolite system in its “bond-prepared” geometry is defined by eq 2b. The sum of the energies for processes (2a) and (2b) gives the adsorption energy of NO. The deformation energies for type I sites of Cu⁺ are in the range 7.0–9.2 kcal/mol, while significantly smaller values (0.8–2.0 kcal/mol) are found for type II sites. This difference between

TABLE 3: Interaction Energies (kcal/mol) and Cu–N Bond Lengths (in Å) of NO Adsorbed on Different Models for Cu⁺ Type II Sites (I2) in MFI^a

zeolite	E_{ads}	$r_{\text{Cu-N}}$
Cu ⁺	30.8	1.934
{Cu3T} _Z	34.8	1.807
Cu3T//{Cu3T} _Z	34.6	1.807
Cu ⁺ //ON{Cu3T} _Z	22.4	(1.807) ^b
CuAl(OH) ₄ //{Cu3T} _Z	35.1	1.807
CuAl(OH) ₄	34.7	1.795
CuAl(OSiH ₃) ₂ (OH) ₂	34.1	1.802
Cu ⁺ (H ₂ O) ₂ //{3T} _Z	30.6	1.850
Cu ⁺ (H ₂ O) ₂	12.6	1.86

^a Corresponding values for gas phase Cu⁺–NO are also given. ^b Not optimized.

deformation energies explains the difference between NO adsorption energies on Cu⁺ ions in type I and type II sites (Table 2).

Numerous computational studies have been made before, reporting Cu⁺···NO interaction energies from 5 to 51 kcal/mol.^{16–18,21–27,45–47} This large variation can be explained by the different methods employed for describing the electronic structure (Hartree–Fock and DFT employing various exchange–correlation functionals) and by the different cluster models adopted. Cluster models such as ON–Cu⁺(H₂O)_{*n*} (*n* = 2–4) and ON–CuAlSi_{*n*}O_{*m*}H_{*k*} (*n* between 0 and 6) were used. Either the structure of these clusters was fully optimized or the initial geometry was taken from crystallographic data of a particular zeolite and a varying number of constraints was applied during the geometry optimization. The suitability of a given method can be easily judged from the results for the Cu⁺–NO gas-phase species. While B3LYP yields binding energies within 1 kcal/mol of the observed value (26.9 ± 1.2 kcal/mol; observed D_0 plus calculated ZPVE, see Table 7)), Hartree–Fock yields much too small values (16.3 kcal/mol)²⁶ and gradient-corrected functionals without Fock exchange such as BP86 yield much too large results (37.6 kcal/mol).¹⁶

The dependence of the adsorption energy on the size and type of the cluster model and on embedding for the I2 site in MFI (type II) is shown in Table 3. The smallest energy reported for the binding of NO onto a Cu–zeolite model (5 kcal/mol)²⁵ is explained by the use of Hartree–Fock and by the constraints imposed on a 4-T_r cluster model,²⁵ which do not allow the Cu⁺ atom to move sufficiently out–off the ring plane. For the (nonconstraint) 1-T model, CuAl(OH)₄, Hartree–Fock yields an NO binding energy of a mere 11.3 kcal/mol compared to the B3LYP result of 34.7 kcal/mol (Table 3). The largest binding energy reported (51 kcal/mol)¹⁶ is clearly overestimated due to the use of the BP86 exchange–correlation functional together with a small basis set. The local density approximation (LDA) yields even larger binding energies for Cu⁺–NO (60 kcal/mol)⁴⁸ and this explains the large ON–CuZ binding energy of 43.3

TABLE 4: NBO Population Analysis and Wiberg Bond Indices for NO at Cu⁺ Type II Site Compared to Gas-Phase Cu⁺–NO

		NBO charges						bond indices	
		O	N	Cu	3d	4s	Z	O–N	N–Cu
ZCuNO ^a	charge	−0.14	−0.05	1.06	9.63	0.30	−0.87	1.94	0.51
	spin	0.38	0.62	0.002			0.0		
Cu ⁺ NO//ZCuNO ^b	charge	0.02	0.00	0.98	9.80	0.20			
	spin	0.37	0.54	0.09					
Cu ⁺ NO ^c	charge	0.02	0.05	0.93	9.85	0.21		2.17	0.30
	spin	0.36	0.52	0.12					
NO; CuZ ^a	charge	−0.18	0.18	0.92	9.92	0.13	−0.92	2.11	
	spin	0.30	0.70	−					

^a 3-T cluster model representing the type II site, Al in T12 position. Geometry optimized at the QM-Pot level. ^b Geometry optimized for ON–CuZ system. ^c Geometry optimized for the gas-phase Cu⁺–NO ion.

kcal/mol reported in ref 18. Unfortunately, comparison was made in that paper with unreliable heats of adsorption¹⁸ derived from temperature-programmed desorption (TPD) of NO,⁴⁹ which are much larger than more recent microcalorimetry data⁵⁰ (see section 5).

Table 3 shows that a model consisting of 3 TO₄ tetrahedra only (3-T) yields for type II sites (but not for type I sites) the same binding energy as an embedded cluster model. Indeed, when the B3LYP functional is used together with a sufficiently flexible basis set for a 3-T zeolite model (as was done in ref 27) the ON–CuZ interaction energies reported are very similar to the result obtained in the present study for type II sites in MFI. Table 3 further shows that even the 1-T cluster model, CuAl(OH)₄, can represent type II sites. However, water molecules as ligands are not valid models of the zeolite environment; only about one-third of the binding energy is obtained (Table 3). Only after fixing the oxygen atoms of the water ligands to positions they would have in the zeolite framework are NO binding energies of the right order of magnitude obtained (30.6 kcal/mol, Table 3). But even these models still fail to reproduce the increase of the binding energy of the Cu⁺ ion in the zeolite compared to the free Cu⁺ ion.

Neither the 3-T nor the 1-T model can describe the strong variation of the NO binding energy with the type of Cu⁺ sites or its variation across different zeolite frameworks (Table 2). Inclusion of the periodic zeolite framework is necessary and this as well as previous studies have demonstrated that the QM-Pot approach applied here is able to describe these variations.

4.2. Charge and Spin Distributions. The results of the NBO analysis⁵¹ for the NO and Cu⁺–NO gas-phase species, for Cu⁺ in the zeolite (type II site, Al at T₁₂) and for the ON–CuZ adsorption complex, are collected in Table 4. For comparison results for the isolated Cu⁺–NO complex at the geometry optimized for the ON–CuZ adsorption complex are also shown. Interaction of the Cu⁺ ion with the zeolite matrix results in partial charge transfer from the zeolite framework to Cu⁺ (0.08 e). As a result, the nature of the NO interaction with the isolated Cu⁺ ion (Cu⁺NO) and with the Cu⁺ ion in a zeolite environment (ON–CuZ) is rather different: there is a significant charge transfer from NO to Cu⁺ in the Cu⁺NO species (0.07 e) while charge flows to NO in ON–CuZ (−0.19 e) and the electron population on the Cu⁺ cation decreases significantly (−0.14 e). The changed character of the Cu⁺•••NO interaction upon the insertion into the zeolite environment is also apparent from the Wiberg's bond index. Its value points to a dominantly electrostatic interaction in the Cu⁺NO gas-phase complex (Wiberg bond index 0.30), but indicates a significant increase in covalency of the Cu–N bond for the ON–CuZ adsorption complex (Wiberg bond index 0.51).

Also the spin population on the Cu⁺ ion changes dramatically when the Cu⁺–NO cation is embedded in the zeolite framework.

TABLE 5: Mulliken Atomic Charges and Spin Populations Calculated for Various Cu⁺ Sites in Zeolites^a

		Mulliken atomic charges				atomic spin populations			
		O	N	Cu	Z ^b	O	N	Cu	Z ^c
FER	I	0.02	−0.03	0.55	−0.50	0.37	0.58	0.045	0.00
	II	0.00	−0.03	0.54	−0.51	0.38	0.61	0.020	−0.01
MFI	I	0.00	−0.02	0.52	−0.50	0.38	0.62	0.015	−0.01
	II	0.00	−0.04	0.56	−0.52	0.38	0.60	0.023	0.00
Cu ⁺ NO//ZCuNO ^d		0.15	0.09	0.76		0.36	0.52	0.12	
(Cu ⁺ NO) _g		0.16	0.09	0.75		0.35	0.49	0.16	
NO; CuZ		−0.02	0.02	0.59	−0.59	0.29	0.71	−	−

^a 3-T cluster models used at the geometries optimized at the QM-Pot level. ^b Overall charge on the cluster representing the zeolite framework. ^c Overall spin density on the cluster representing the zeolite framework. ^d Geometry optimized for the ON–CuZ system (site I2, MFI).

The Cu⁺NO gas-phase complex shows significant spin population on Cu⁺ (0.12 e), which upon insertion into the zeolite environment is reduced to 0.002 e. It is shifted from Cu⁺ to the N atom. Calculations for Cu⁺–NO at the structure of the ON–CuZ adsorption complex show that the changes of the electron and spin populations between the gas-phase Cu⁺NO and the ON–CuZ adsorption complex are partially due to geometry changes (reduced Cu–N bond distance and increased CuNO bond angle, Table 2), but the presence of the zeolite framework has the dominant effect.

Table 5 shows Mulliken atomic charges and spin populations for NO adsorbed at type I and type II sites in MFI and FER. Mulliken-type population analysis is more commonly applied because it is computationally less demanding. However, the NBO analysis provides more reliable information about the charge distribution, not depending strongly on the basis set used. For the NO complex with the MFI type II site the NBO results (Table 4) and the Mulliken results (Table 5) can be directly compared. The Mulliken charges on Cu, notably in the zeolite, are much smaller than the NBO charges which are close to 1. Qualitatively different changes are found for the electron population on Cu⁺ in the zeolite upon interaction with NO. The electron population on the Cu⁺ ion increases by 0.03 e according to the Mulliken analysis, while it decreases significantly (−0.14 e) when the NBO analysis is applied. Table 5 shows Mulliken charge and spin distributions of various Cu⁺ sites in zeolites MFI and FER. We conclude that the subtle differences in the local structure of the different sites only marginally affect the electron distribution and this is confirmed by the hyperfine coupling constants.

4.3. Hyperfine Coupling Constants. Calculated HFCC for NO adsorbed on one specific Cu⁺ site of each type in MFI, Z6 for type I and I2 for type II, are reported in Table 6. The calculations for type II site (I2) are made for a 7-T model at the structure optimized for the embedded 3-T model. Compared

TABLE 6: Calculated A_{iso} and Anisotropic Component of the shf Tensor (in 10^{-4} cm^{-1}) Calculated for Gas-Phase Cu⁺NO Ion and for ON–CuMFI Complexes at the B3LYP/BS1 Level

		II(I2)site Al in T12	I(Z6) site Al in T4	experiment		
	Cu ⁺ NO	7-T/3-T ^a	6-T _r ^b	ref 52	ref 54	
					A	B
<i>A</i> ₀ (Cu)	503.6	148.9	137.6	159	168	177
<i>T</i> _x	10.6	26.8	26.8	23	48	65
<i>T</i> _y	−4.1	−4.9	−4.1	−9	−10	−19
<i>T</i> _z	−6.5	−21.9	−22.7	−14	−38	−47
<i>A</i> ₁ (N) ^c	30.4	29.8	29.3	28	29	29

^a Geometry optimized at the QM-Pot level using 3-T embedded cluster. ^b Geometry optimized at the QM-Pot level using 6-T embedded cluster. ^c The largest value of nitrogen hyperfine tensor corresponding to the direction determined by the 2π singly occupied orbital.

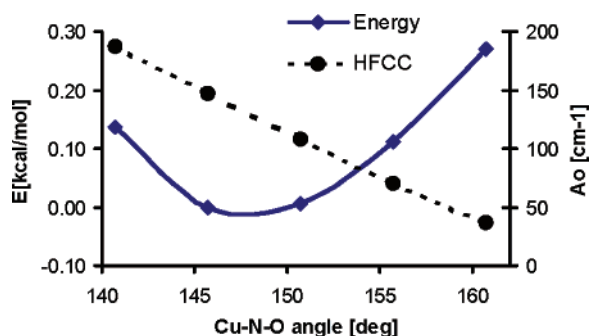


Figure 4. Dependence of A_0 ($\text{cm}^{-1} \times 10^{-4}$) and the energy on the CuNO bond angle. Calculations carried out with the 3-T cluster model at the geometry optimized at the QM-Pot level for type II site (Al in T12 position).

to calculations directly on the 3-T model (shown in Table 1, B3LYP), changes of less than $2 \times 10^{-4} \text{ cm}^{-1}$ are observed. For the type I site (Z6) the 6-T_r model has been used at the structure optimized for the embedded 6-T_r model. Comparison can be made with the values for the Cu⁺–NO gas-phase complex, also shown in Table 6. The largest component of the ¹⁴N hyperfine tensor (corresponding to the direction of singly occupied $2\pi^*$ orbital) does not change between the gas-phase Cu⁺–NO species and NO adsorbed on different Cu⁺ sites in zeolites. It is in a good agreement with experimental values.^{52–54}

Both A_0 and the anisotropic components of the superhyperfine (shf) tensor on Cu, T_x , T_y , and T_z , differ significantly between Cu⁺–NO and the ON–CuZ adsorption complexes. This is not unexpected, as the population analysis has already indicated a significant decrease of the spin population from the gas-phase Cu⁺–NO complex to the ON–CuZ adsorption complexes. Changes in the Cu⁺ coordination (geometry) between the two adsorption sites leave the anisotropic shf tensor components relatively unaffected. Therefore, further discussion will focus on the isotropic constant A_0 , which differs by $11.3 \times 10^{-4} \text{ cm}^{-1}$ between the two adsorption structures.

To analyze the origin of the difference, the dependence of A_0 on the N–O distance, the Cu–N distance, and the Cu–N–O angle is calculated for the 3-T model of the type II (I2) site. Over a range of Cu–N distances found in zeolites, 1.80–1.82 Å (Table 2), the calculated A_0 values change by about $3.3 \times 10^{-4} \text{ cm}^{-1}$. The variation of the N–O distances in Table 2 are so small (between 1.158 and 1.161 Å) that A_0 changes by less than $1 \times 10^{-4} \text{ cm}^{-1}$. By far the strongest effect on A_0 is found for the Cu–N–O angle (Figure 4). When this angle changes by 5°, which is achieved at almost no energy change (0.1 kcal/mol, Figure 4), A_0 changes by $40 \times 10^{-4} \text{ cm}^{-1}$. The calculated A_0 difference between Cu⁺–NO complexes at type I and type

II sites (148.9 and $137.6 \times 10^{-4} \text{ cm}^{-1}$, respectively) are mainly due to the change of Cu–N–O angle (145.7 and 148.5°, respectively). A realistic estimate even of the A_0 difference between two different adsorption complexes would require calculation of vibrationally and thermally averaged A_0 parameters. However, given the flatness of the potential energy surface for the Cu–N–O angle, possible interactions of NO with the framework atoms on the opposite side of the wall of the zeolite channel need to be taken into account. The importance of such interactions was shown recently for the CO–Cu⁺/MFI system.⁴⁴

Given the large dependence on the exchange-correlation functional used and the high sensitivity to the orientation of the adsorbed NO molecule relative to the zeolite surface, we feel that a better agreement between calculated and observed HFCC parameters than seen in Table 6 cannot be expected. We conclude that presently it cannot be decided if the HFCC parameters observed by Sojka et al.⁵² and recently confirmed by Prestipino et al.,⁵³ $A_0 = 159 \times 10^{-4} \text{ cm}^{-1}$, are due to type I and type II sites. Pöppel et al. have identified two paramagnetic species from additional Q-band and W-band ESR measurements,⁵⁴ which differ in one component of the hfc tensor, but not in the other two. This leads to different isotropic values (A_0 values of 168 and $177 \times 10^{-4} \text{ cm}^{-1}$), but also to very different anisotropic tensor components T_x , T_y , and T_z . This, however, is very unlikely because the calculated anisotropic component values are neither sensitive to the method (Table 1) nor to changes of the geometry between different sites (Table 6). Thus, despite the similar difference between the calculated isotropic values for sites II(I2) and I(Z6), $11 \times 10^{-4} \text{ cm}^{-1}$, and between the observed isotropic values for species A and B, $8 \times 10^{-4} \text{ cm}^{-1}$, our calculations do not confirm the assignment of the two different species A and B to ON–CuZ adsorption complexes on type I and type II sites in Cu–zeolites.

5. Discussion

5.1. Structure and Energies of NO Adsorbed on Different Cu⁺ Sites in Zeolites. When NO interacts with extraframework Cu⁺ ions in zeolites, a mononitrosyl complex is formed in which Cu⁺ is coordinated to the nitrogen atom of NO and to two framework oxygen atoms of a single AlO₄ tetrahedron (Figure 2). The same Cu⁺ ion coordination was found for NO complexes with all types of Cu⁺ sites in both MFI and FER zeolites. Thus, the coordination number of Cu⁺ decreases or increases depending on the original Cu⁺ site type. When Cu⁺ is coordinated to three or four framework oxygen atoms in type I sites (at the wall of the channel), upon interaction with NO it loses the coordination to oxygen atoms, which do not belong to the AlO₄ tetrahedron. On the contrary, when Cu⁺ is coordinated to two oxygen atoms of a single AlO₄ tetrahedron in type II sites (channel intersection), the coordination to framework atoms does not change upon the interaction with NO. The same behavior was found for various small molecules (CO, N₂, NO₂, and H₂O) previously.⁴⁵ The changes in Cu⁺ coordination upon the adsorption of CO were theoretically investigated recently¹⁴ and good agreement with experimental EXAFS results was found.⁵⁵

In accordance with the similar structures of the adsorption complexes for type I and type II sites, the anisotropic components of the Cu⁺ shf tensor calculated for type I and type II sites in MFI are very similar and the isotropic values, A_0 , show only a small difference (138 and $149 \times 10^{-4} \text{ cm}^{-1}$, respectively), which reflects a Cu–N–O bond angle difference of less than 3°. Despite the presence of two distinct copper sites (Cu²⁺) in the parent sample, Sojka et al. found only a single Cu⁺NO

TABLE 7: Comparison of Calculated Binding Energies (Corrected for BSSE), $E_{\text{int}}^{\text{BSSE}}$, and Binding Energies at 0 K, D_0 , with Observed Data

		$E_{\text{int}}^{\text{BSSE}}$ ^a	D_0	obsd
Cu ⁺ CO		36.9	35.4	35.5 ± 1.6 (D_0) ^b
OC–CuMFI	II(I2)	35.1	33.2	ca. 31 (q_a) ^c
	I(Z6)	28.6	26.3	
Cu ⁺ NO		27.3	26.5	26.1 ± 1.2 (D_0) ^d
ON–CuMFI	II(I2)	29.5	28.6	ca. 24 (q_a) ^c
	I(Z6)	22.3	21.4	

^a BSSE correction included. ^b D_0 , ref 59. ^c Heats of adsorption at 303 K, ref 50. ^d D_0 , ref 5.

species in their EPR spectra.⁵² The shf tensor elements reported and recently confirmed by Prestipino et al.⁵³ are in reasonable agreement with the calculated values. However, it cannot be decided if the observed EPR spectra are due to the more stable complexes at sites II only or if also type I sites contribute to the signal. While the isotropic values, A_0 , depend on the method (functional) and the site type, the results for the anisotropic components are stable. Based on the anisotropic values, we cannot support the assignment of species A and B found by Pöppl and Hartmann⁵⁴ in high-frequency W-band ESR spectra to two different types of ON–CuZ complexes in Cu–MFI. We note that it will be difficult for any characterization method to provide evidence for two different types of adsorption complexes because—as explained above—the adsorption complexes are very similar, even if the Cu⁺ sites have been different before adsorption. On the contrary, relatively large differences in adsorption energies were found.

5.2. Adsorption Energies. Table 7 compares calculated bond dissociation energies (for the gas-phase species) and heats of adsorption (for Cu zeolites) with available observed values. The Cu⁺–NO bond dissociation energy was measured recently (D_0 , 26.1 ± 1.2 kcal/mol) and comparison was made with CCSD(T) (23.5 kcal/mol) and B3LYP (27.0 kcal/mol) results.⁵ The present B3LYP calculations yield a bond dissociation energy (26.5 kcal/mol) which is within the experimental error bars. This is also true for the Cu⁺–CO gas-phase complex. Our calculations show that the Cu⁺–NO and Cu⁺–CO interactions are modified when the Cu⁺ is in a zeolite. For type I sites in MFI and FER the NO interaction is up to 5 and 11 kcal/mol, respectively, weaker than that for naked Cu⁺ ions. On the contrary, the Cu⁺···NO interaction can be up to 2.2 kcal/mol larger for Cu⁺ ions in type II sites in MFI. For CO, binding to type II sites is also by 6 kcal/mol stronger than to type I sites, but even type II sites bind CO less strongly than gas-phase Cu⁺ ions. Neither the strong dependence of the Cu⁺···NO interaction energy on the type of the Cu⁺ site nor its variation across different zeolite frameworks (Table 2) can be obtained from calculations on nonembedded cluster models such as the 3-T or 1-T models. Only calculations that include the full periodic framework and its relaxation such as embedded cluster calculations by the QM-Pot approach as applied in this study are able to describe these variations.

The heats of adsorption of NO and CO on Cu-exchanged MFI (ZSM-5) have been measured by microcalorimetry.⁵⁰ The differential heats as a function of the NO uptake show plateaus for low loading at about 31 kcal/mol for CO and 24 kcal/mol for NO. The value for CO is in good agreement with the estimate from the present calculations (33 and 26 kcal/mol for sites type II and I, respectively). Calculated value for NO interaction with Cu⁺ in type II is 5.5 kcal/mol above the experiment, while for type I site calculations are 1.7 kcal/mol below the experiment. Our comparison of calculated D_0 and measured q_a assumes that

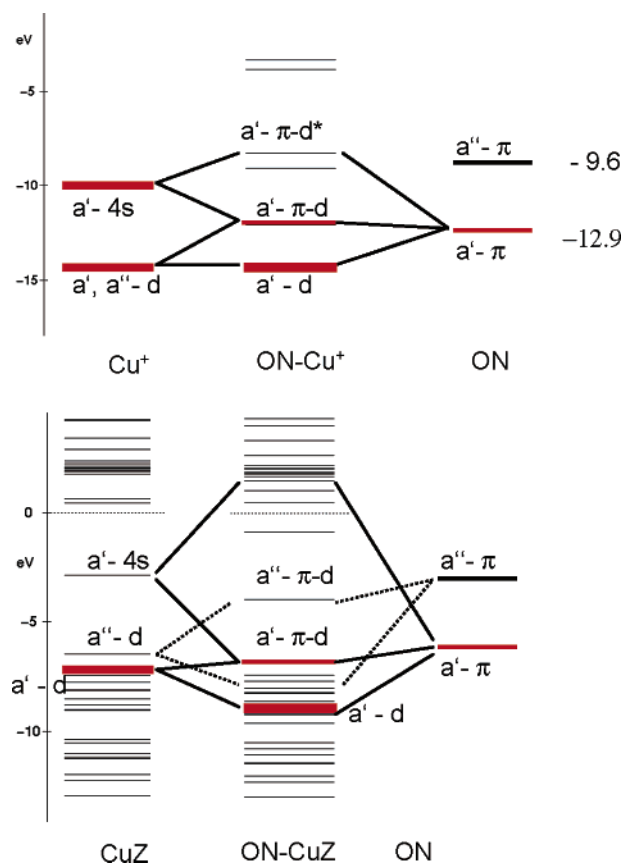


Figure 5. MO correlation diagrams for the ON–Cu⁺ gas-phase complex (top) and the ON–CuZ adsorption complex (bottom, Z – shell-1.5 model). In the top diagram the NO orbital energies are given for NO in the potential of a point charge at the position of Cu⁺ ion in the ON–Cu⁺ gas-phase complex. For systems with open-shell electronic structures the α -spin orbital energies are shown.

all thermal contributions to the heat of adsorption cancel to a large extent. In a previous computational study¹⁸ heats of adsorption as large as 43.9–49.5 kcal/mol have been derived by applying the Redhead equation to data of Li and Armor⁴⁹ for temperature-programmed desorption (TPD) of NO from CuMFI. Comparison with the direct microcalorimetric measurements⁵⁰ and the present calculations shows that these values are very unreliable, which is frequently the case for equilibrium data derived from nonequilibrium measurements. Heats of NO adsorption as low as 12 kcal/mol and lower have also been reported for CuMFI.⁵⁶ Possible explanations are that this catalyst may not have the isolated Cu⁺/AlO₄[−] sites studied here (we note that a rather overexchanged Cu/MFI sample, 2.9 wt % of Al₂O₃ and 6.5 wt % of Cu, was used) or that the multisite Langmuir model used to fit the adsorption isotherms is not appropriate.

5.3. Nature of the Cu⁺···NO Interaction. The interaction of Cu⁺ ion with zeolite framework changes the Cu⁺ ion ability to bind other ligands. Even if the Cu⁺···NO interaction energy does not change much between gaseous and embedded copper species (for type II sites on the intersection) the character of the interaction changes significantly. The different character of ON···Cu⁺ interaction in the Cu⁺–NO gas-phase complex and the ON–CuZ adsorption complex can also be discussed in terms of the MO diagram (Figure 5). As noted before by Yokumichi,¹⁶ the a' -SOMO of Cu⁺–NO results from a bonding interaction of the a' -SOMO of NO with the occupied a' -d-orbitals of Cu⁺ and the empty 4s orbital of Cu⁺. This leads to a charge transfer of 0.07 e and to a spin transfer of 0.12 e to Cu⁺ (NBO analysis,

Table 4). Note that opening of the d-shell on Cu^+ (3d–4s hybridization) is a prerequisite to this charge transfer because the 3d orbitals are fully occupied in Cu^+ . This is illustrated by the occupations of the Cu 3d (9.85) and Cu 4s (0.21) orbitals in $\text{Cu}^+ - \text{NO}$. Since the SOMO of NO is antibonding, depopulation of this MO by partial electron transfer to Cu^+ makes the NO bond in the $\text{Cu}^+ - \text{NO}$ gas-phase complex stronger (Wiberg bond index 2.17) than that in the NO radical (Wiberg bond index 2.11). This is the reason for a shorter NO bond (by 0.014 Å) and a higher vibrational wavenumber (by 18 cm^{-1}) in the $\text{Cu}^+ - \text{NO}$ complex.

Rather different MO interactions are seen in the MO diagram for the ON–CuZ system. For easier following of the different interactions, we show the results for the shell-1.5 model of CuZ, $\text{CuAl}(\text{OH})_2(\text{OSiH}_3)_2$, which has C_s symmetry and is a small, but perfect model for the I2 site.⁸ The a' -SOMO of the ON–CuZ complex results from the same orbital interactions ($a' - \pi$ -SOMO of NO, $a' - 3d$ and $a' - 4s$ of CuZ) as seen in the gas-phase complex, but the effect is stronger. The 4s population becomes larger (0.30) and the 3d population even smaller (9.63). The reason is a cooperative effect between ON– Cu^+ and $\text{Cu}^+ - \text{zeolite}$ framework interaction. The closed shell 3d¹⁰ ion Cu^+ binds to the zeolite framework basically by electrostatic interactions. This attractive interaction is counteracted by exchange repulsion between the 3d¹⁰ shell on Cu^+ and the nonbonded electron pairs on the zeolite oxygen atoms. The Cu^+ ion can get closer to the zeolite framework only if it partially opens its d-shell. This is indeed the case as we see from the 4s population of 0.13 e in the CuZ system (Table 4). Another indication of the “activation” of the Cu^+ ion in the zeolite is the 3d–4s excitation energy, which is 2.47 eV in the naked Cu^+ ion and 1.93 eV for Cu^+ in the type II site (excitation into the triplet state, B3LYP/DZP calculation for the Cu-shell-1.5 model). In the ON–CuZ complex both the ON– Cu^+ and the $\text{Cu}^+ - \text{Z}^-$ interactions profit from the d–s hybridization, but can share the costs. The increase in the strength of both interactions in the ON–CuZ adsorption complex is also seen in the structure. Not only does the N–Cu distance shrink (1.807 compared to 1.934 in the ON– Cu^+ gas-phase complex), but also the Cu–O(zeolite) distances are smaller in the ON–CuZ adsorption complex (2.02, 2.04 Å) than in the CuZ site (2.04, 2.05 Å).

The existence of a cooperative effect is also seen in the interaction energy. The total interaction energy of the ON–CuZ adsorption complex with respect to the three isolated components (NO, Cu^+ , Z^-) is 218.7 kcal/mol, while the sum of all pair interactions is 207.0 kcal/mol. (All energies calculated at the geometry of the ON–CuZ adsorption complex for the embedded 3T model of the MFI I2 site, Al at T12.) Hence, there is a three-body effect in the stabilization energy of 11.7 kcal/mol.

If the orbital interactions involving the SOMO orbital were the only relevant interactions, we would expect an even stronger charge (and spin) transfer from NO to Cu^+ and an even stronger NO bond. This is not the case as we know from Table 4. The Wiberg bond index of 1.94 indicates that the NO bond in the ON–CuZ adsorption complex is not only weaker than in the $\text{Cu}^+ - \text{NO}$ gas-phase complex (2.17) but also even weaker than in free NO (2.11). The reason is that the repulsive interactions between the closed 3d shell on Cu^+ and the nonbonding orbitals on the zeolite O atoms push the d-orbitals so much up that the 3d a'' orbitals (HOMO in CuZ) can effectively interact with the a'' -LUMO of NO. This additional orbital interaction between Cu^+ and NO is reflected by a larger Wiberg bond index for the Cu–N bond, 0.51 compared to 0.30 for the $\text{Cu}^+ - \text{NO}$ ion. The

Cu–NO bonding combinations in the a'' subspace stabilize the occupied orbitals, which causes charge transfer in the opposite direction, from Cu 3d into the LUMO of NO. The partial occupation of the a'' -LUMO of NO (which is also antibonding) is obviously larger than the partial depopulation of the a' -SOMO of NO so that the net effect is a transfer of 0.19 e to NO. Since these electrons go into antibonding NO orbitals, this results in a Wiberg bond index of 1.94 for the NO bond—smaller than that for the NO radical itself. Evidence for the increase of the N–O bond strength in the $\text{Cu}^+ - \text{NO}$ gas-phase complex due to depopulation of the antibonding SOMO of NO and for the weakening of the N–O bond in the ON–CuZ adsorption complex due to population of the antibonding LUMO of NO comes also from the NO bond distances and the NO vibrational frequencies; see Table 2.

Even stronger changes between binding to gas-phase Cu^+ ions and to Cu^+ ions in zeolite MFI (I2 site, type II) were previously found by Rodriguez-Santiago et al. for NO_2 .⁸ They used the shell-1.5 cluster model and showed that this model yields results for the I2 site that are virtually identical with embedded cluster results obtained with the combined QM-Pot technique. A similar explanation was found; 3d–4s promotion on Cu^+ leads to a more favorable orbital interaction between NO_2 and Cu^+ and at the same time reduces the repulsion between Cu^+ and the zeolite framework. The nature of the NO interaction with Cu^+ ion was also discussed in ref 57.

6. Conclusions

The present study revealed the critical role of the zeolite environment in activating Cu^+ ions for binding NO molecules and for weakening the NO bond. The structures of the NO adsorption complexes are very similar for different framework types (MFI and FER) and for different types of sites (Type I and type II) and spectroscopies will hardly be able to differentiate between adsorption complexes at different sites. What distinguishes type II from type I sites is the coordination of Cu^+ to the zeolite framework before the interaction with NO and the geometry and the amount of (deformation) energy needed to create the structure prepared for binding NO. Hence, the difference between the different sites is not in the properties of the ON–CuZ adsorption complex (as the similar NO stretching frequency shifts and the similar hyperfine coupling constants show), but in how much heat of adsorption is released on binding the NO. Adsorption can affect the overall kinetics of a catalytic process, and instead of the intrinsic barrier of the rate-determining step, the apparent barrier, $\Delta E_{\text{app}} = \Delta E_{\text{intrinsic}} - q_a$, may determine the overall rate. Since the heat of adsorption is by 6.5–7.2 kcal/mol lower for type I sites, rates could be 5 orders of magnitude smaller for conversions at type I sites (at room temperature). The detailed mechanism of the NO decomposition is not yet fully understood, but if isolated Cu^+ sites play a crucial role among the different sites available, conversions at type II sites would be much faster than those at type I sites.

Acknowledgment. This work was supported by a Grant of the Ministry of Education of the Czech Republic (Project No. LN00A032, Center for Complex Molecular Systems and Biomolecules) and by Deutsche Forschungsgemeinschaft. Thanks go also to Marek Sierka for the QM-Pot program and to Julian Gale for providing the GULP program.

References and Notes

- (1) Ryder, J. A.; Chakraborty, A. K.; Bell, A. T. *J. Catal.* **2003**, 220, 84.

- (2) Schroder, D.; Fiedler, A.; Schwarz, J.; Schwarz, H. *Inorg. Chem.* **1994**, *33*, 5094.
- (3) Iwamoto, M.; Furukawa, H.; Mine, Y.; Uemura, F.; Mikuriya, S.; Kagawa, S. *J. Chem. Soc., Chem. Commun.* **1986**, 1272.
- (4) Giamello, E.; Murphy, D. M.; Magnacca, G.; Morterra, C.; Shioya, Y.; Nomura, T.; Anpo, M. *J. Catal.* **1992**, *136*, 510.
- (5) Koszinowski, K.; Schroder, D.; Schwarz, H.; Holthausen, M. C.; Sauer, J.; Koizumi, H.; Armentrout, P. B. *Inorg. Chem.* **2002**, *41*, 5882.
- (6) Ruggiero, C. E.; Carrier, S. M.; Antholine, W. E.; Whittaker, J. W.; Cramer, C. J.; Tolman, W. B. *J. Am. Chem. Soc.* **1993**, *115*, 11285.
- (7) Schneider, J. L.; Carrier, S. M.; Ruggiero, C. E.; Young, V. G.; Tolman, W. B. *J. Am. Chem. Soc.* **1998**, *120*, 11408.
- (8) Rodríguez-Santiago, L.; Sierka, M.; Branchadell, V.; Sodupe, M.; Sauer, J. *J. Am. Chem. Soc.* **1998**, *120*, 1545.
- (9) Wichterlova, B.; Dedecek, J.; Sobalik, Z.; Vondrova, A.; Klier, K. *J. Catal.* **1997**, *169*, 194.
- (10) Lamberti, C.; Bordiga, S.; Salvalaggio, M.; Spoto, G.; Zecchina, A.; Geobaldo, F.; Vlaic, G.; Bellatreccia, M. *J. Phys. Chem. B* **1997**, *101*, 344.
- (11) Kumashiro, P.; Kuroda, Y.; Nagao, M. *J. Phys. Chem. B* **1999**, *103*, 89.
- (12) Nachtigall, P.; Davidova, M.; Nachtigallova, D. *J. Phys. Chem. B* **2001**, *105*, 3510.
- (13) Nachtigallova, D.; Nachtigall, P.; Sierka, M.; Sauer, J. *Phys. Chem. Chem. Phys.* **1999**, *1*, 2019.
- (14) Davidova, M.; Nachtigallova, D.; Bulanek, R.; Nachtigall, P. *J. Phys. Chem. B* **2003**, *107*, 2327.
- (15) Sauer, J.; Nachtigallova, D.; Nachtigall, P. In *Catalysis by Unique Metal Ion Structures in Solid Matrices. From Science to Application*; Centi, G., Wichterlova, B., Bell, A. T., Eds.; Kluwer: Dordrecht, 2001; Vol. 13, p 221.
- (16) Yokomichi, Y.; Yamabe, T.; Ohtsuka, H.; Kakumoto, T. *J. Phys. Chem.* **1996**, *100*, 14424.
- (17) Schneider, W. F.; Hass, K. C.; Ramprasad, R.; Adams, J. B. *J. Phys. Chem. B* **1998**, *102*, 3692.
- (18) Trout, B. L.; Chakraborty, A. K.; Bell, A. T. *J. Phys. Chem.* **1996**, *100*, 17582.
- (19) Solans-Monfort, X.; Branchadell, V.; Sodupe, M. *J. Phys. Chem. A* **2000**, *104*, 3225.
- (20) Solans-Monfort, X.; Branchadell, V.; Sodupe, M. *J. Phys. Chem. B* **2002**, *106*, 1372.
- (21) Pietrzyk, P.; Piskorz, W.; Sojka, Z.; Broclawik, E. *J. Phys. Chem. B* **2003**, *107*, 6105.
- (22) Hass, K. C.; Schneider, W. F. *Phys. Chem. Chem. Phys.* **1999**, *1*, 639.
- (23) Schneider, W. F.; Hass, K. C.; Ramprasad, R.; Adams, J. B. *J. Phys. Chem. B* **1997**, *101*, 4353.
- (24) Zhanpeisov, N. U.; Ju, W. S.; Matsuoka, M.; Anpo, M. *Struct. Chem.* **2003**, *14*, 247.
- (25) Zhanpeisov, N. U.; Nakatsuji, H.; Hada, M.; Nakai, H.; Anpo, M. *Catal. Lett.* **1996**, *42*, 173.
- (26) Yokomichi, Y.; Ohtsuka, H.; Tabata, T.; Okada, O.; Yokoi, Y.; Ishikawa, H.; Yamaguchi, R.; Matsui, H.; Tachibana, A.; Yamabe, T. *Catal. Today* **1995**, *23*, 431.
- (27) Tajima, N.; Hashimoto, M.; Toyama, F.; El-Nahas, A. M.; Hirao, K. *Phys. Chem. Chem. Phys.* **1999**, *1*, 3823.
- (28) Sierka, M.; Sauer, J. *J. Chem. Phys.* **2000**, *112*, 6983.
- (29) Lee, C.; Yang, W.; Parr, R. G. *Phys. Rev. B: Condens. Matter* **1988**, *37*, 785.
- (30) Becke, A. D. *J. Chem. Phys.* **1993**, *98*, 5648.
- (31) Schafer, A.; Horn, H.; Ahlrichs, R. *J. Chem. Phys.* **1992**, *97*, 2571.
- (32) Dick, B. G.; Overhauser, A. W. *Phys. Rev.* **1958**, *112*, 90.
- (33) Sierka, M.; Sauer, J. *Faraday Discuss.* **1997**, 41.
- (34) Rappe, A. K.; Casewit, C. J.; Colwell, K. S.; Goddard, W. A.; Skiff, W. M. *J. Am. Chem. Soc.* **1992**, *114*, 10024.
- (35) Treutler, O.; Ahlrichs, R. *J. Chem. Phys.* **1995**, *102*, 346.
- (36) Gale, J. D.; Rohl, A. L. *Mol. Simul.* **2003**, *29*, 291.
- (37) Munzarova, M.; Kaupp, M. *J. Phys. Chem. A* **1999**, *103*, 9966.
- (38) Freysoldt, C.; Poppl, A.; Reinhold, J. *J. Phys. Chem. A* **2004**, *108*, 1582.
- (39) Munzarova, M. L.; Kubacek, P.; Kaupp, M. *J. Am. Chem. Soc.* **2000**, *122*, 11900.
- (40) Pyykko, P.; Pajanne, E.; Inokuti, M. *Int. J. Quantum Chem.* **1973**, *7*, 785.
- (41) Carpenter, J. E.; Weinhold, F. *Theochem-J. Mol. Struct.* **1988**, *46*, 41.
- (42) Frisch, M. J.; Trucks, G. W.; Schlegel, H. B.; Scuseria, G. E.; Robb, M. A.; Cheeseman, J. R.; Montgomery, J. A., Jr.; Vreven, T.; Kudin, K. N.; Burant, J. C.; Millam, J. M.; Iyengar, S. S.; Tomasi, J.; Barone, V.; Mennucci, B.; Cossi, M.; Scalmani, G.; Rega, N.; Petersson, G. A.; Nakatsuji, H.; Hada, M.; Ehara, M.; Toyota, K.; Fukuda, R.; Hasegawa, J.; Ishida, M.; Nakajima, T.; Honda, Y.; Kitao, O.; Nakai, H.; Klene, M.; Li, X.; Knox, J. E.; Hratchian, H. P.; Cross, J. B.; Adamo, C.; Jaramillo, J.; Gomperts, R.; Stratmann, R. E.; Yazyev, O.; Austin, A. J.; Cammi, R.; Pomelli, C.; Ochterski, J. W.; Ayala, P. Y.; Morokuma, K.; Voth, G. A.; Salvador, P.; Dannenberg, J. J.; Zakrzewski, V. G.; Dapprich, S.; Daniels, A. D.; Strain, M. C.; Farkas, O.; Malick, D. K.; Rabuck, A. D.; Raghavachari, K.; Foresman, J. B.; Ortiz, J. V.; Cui, Q.; Baboul, A. G.; Clifford, S.; Cioslowski, J.; Stefanov, B. B.; Liu, G.; Liashenko, A.; Piskorz, P.; Komaromi, I.; Martin, R. L.; Fox, D. J.; Keith, T.; Al-Laham, M. A.; Peng, C. Y.; Nanayakkara, A.; Challacombe, M.; Gill, P. M. W.; Johnson, B.; Chen, W.; Wong, M. W.; Gonzalez, C.; Pople, J. A. *Gaussian 03*, R. A.; Gaussian, Inc.: Pittsburgh, PA, 2003.
- (43) Wichterlova, B.; Sobalik, Z.; Dedecek, J. *Catal. Today* **1997**, *38*, 199.
- (44) Bludsky, O.; Silhan, M.; Nachtigallova, D.; Nachtigall, P. *J. Phys. Chem. A* **2003**, *107*, 10381.
- (45) Nachtigall, P.; Davidova, M.; Silhan, M.; Nachtigallova, D. *Stud. Surf. Sci. Catal.* **2002**, *142*, 101.
- (46) Brand, H. V.; Redondo, A.; Hay, P. J. *J. Phys. Chem. B* **1997**, *101*, 7691.
- (47) Schneider, W. F.; Hass, K. C.; Ramprasad, R.; Adams, J. B. *J. Phys. Chem.* **1996**, *100*, 6032.
- (48) Nachtigallova, D.; Davidova, M.; Nachtigall, P. *Collect. Czech. Chem. Commun.* **1998**, *63*, 1202.
- (49) Li, Y.; Armor, J. N. *Appl. Catal.* **1991**, *76*, L1.
- (50) Gervasini, A.; Picciau, C.; Auroux, A. *Microporous Mesoporous Mater.* **2000**, *35–6*, 457.
- (51) Reed, A. E.; Curtiss, L. A.; Weinhold, F. *Chem. Rev.* **1988**, *88*, 899.
- (52) Sojka, Z.; Che, M.; Giamello, E. *J. Phys. Chem. B* **1997**, *101*, 4831.
- (53) Prestipino, C.; Berlier, G.; Xamena, F.; Spoto, G.; Bordiga, S.; Zecchina, A.; Palomino, G. T.; Yamamoto, T.; Lamberti, C. *Chem. Phys. Lett.* **2002**, *363*, 389.
- (54) Poppl, A.; Hartmann, M. *Stud. Surf. Sci. Catal.* **2002**, *142*, 375.
- (55) Zecchina, A.; Bordiga, S.; Palomino, G. T.; Scarano, D.; Lamberti, C.; Salvalaggio, M. *J. Phys. Chem. B* **1999**, *103*, 3833.
- (56) Carniti, P.; Gervasini, A.; Ragaini, V. *J. Chem. Soc., Faraday Trans.* **1997**, *93*, 1641.
- (57) Thomas, J. L. C.; Bauschlicher, C. W.; Hall, M. B. *J. Phys. Chem. A* **1997**, *101*, 8530.
- (58) Scott, A. P.; Radom, L. *J. Phys. Chem.* **1996**, *100*, 16502.
- (59) Meyer, F.; Chen, Y. M.; Armentrout, P. B. *J. Am. Chem. Soc.* **1995**, *117*, 4071.